Evolution of Rev7 interactions in eukaryotic TLS DNA polymerase Polζ

Received for publication, July 14, 2022, and in revised form, December 22, 2022 Published, Papers in Press, December 31, 2022,
https://doi.org/10.1016/j.jbc.2022.102859

Kerry Silva McPherson[1], Alessandro A. Rizzo[1], Heidi Erlandsen[2], Nimrat Chatterjee[3], Graham C. Walker[4], and Dmitry M. Korzhnev[1,*]

From the [1]Department of Molecular Biology and Biophysics, University of Connecticut Health Center, Farmington, Connecticut, USA; [2]Center for Open Research Resources & Equipment, University of Connecticut, Storrs, Connecticut, USA; [3]Department of Microbiology and Molecular Genetics, University of Vermont, Burlington, Vermont, USA; [4]Department of Biology, Massachusetts Institute of Technology, Cambridge, Massachusetts, USA

Edited by Patrick Sung

Translesion synthesis (TLS) DNA polymerase Polζ is crucial for the bypass replication over sites of DNA damage. The Rev7 subunit of Polζ is a HORMA (Hop1, Rev7, Mad2) protein that facilitates recruitment of Polζ to the replication fork *via* interactions with the catalytic subunit Rev3 and the translesion synthesis scaffold protein Rev1. Human Rev7 (hRev7) interacts with two Rev7-binding motifs (RBMs) of hRev3 by a mechanism conserved among HORMA proteins whereby the safety-belt loop of hRev7 closes on the top of the ligand. The two copies of hRev7 tethered by the two hRev3-RBMs form a symmetric head-to-head dimer through the canonical HORMA dimerization interface. Recent cryo-EM structures reveal that *Saccharomyces cerevisiae* Polζ (scPolζ) also includes two copies of scRev7 bound to distinct regions of scRev3. Surprisingly, the HORMA dimerization interface is not conserved in scRev7, with the two scRev7 protomers forming an asymmetric head-to-tail dimer with a much smaller interface than the hRev7 dimer. Here, we validated the two adjacent RBM motifs in scRev3, which bind scRev7 with affinities that differ by two orders of magnitude and confirmed the 2:1 stoichiometry of the scRev7:Rev3 complex in solution. However, our biophysical studies reveal that scRev7 does not form dimers in solution either on its own accord or when tethered by the two RBMs in scRev3. These findings imply that the scRev7 dimer observed in the cryo-EM structures is induced by scRev7 interactions with other Polζ subunits and that Rev7 homodimerization *via* the HORMA interface is a mechanism that emerged later in evolution.

Translesion synthesis (TLS) is a DNA damage tolerance pathway that employs low-fidelity specialized DNA polymerases to copy over DNA lesions, thereby rescuing stalled replication forks or filling single-strand DNA gaps left after replication (1–3). The replicative bypass of many of DNA lesions is executed in a two-step manner in the process of Rev1/Polζ-dependent TLS (4–6). First, Rad6/Rad18-dependent monoubiquitination of the sliding clamp PCNA (7–9) promotes recruitment of the inserter Y-family TLS polymerases (Rev1, Polη in *S. cerevisiae* or Rev1, Polη, Polι, Polκ in humans) that insert nucleotides across the site of DNA damage. Second, the extender B-family TLS polymerase Polζ continues replication of the lesion-distorted DNA primer-template (4–6).

In addition to TLS, Polζ is employed in other cellular pathways to relieve various replication stresses and avert genome instability (10–18). Despite the importance of Polζ in TLS and other pathways, its subunit and structural organization has long remained elusive, creating a gap in our understanding of Polζ regulation and function (19–26). *S. cerevisiae* Polζ (scPolζ) was first described as a complex of the catalytic subunit scRev3 and the accessory subunit scRev7, which increases scRev3 activity by 20- to 30-fold (27, 28). Subsequent studies revealed two additional subunits Pol31:Pol32 in scPolζ (21) and PolD2:PolD3 in human Polζ (hPolζ) (24, 25) that are also subunits of the replicative DNA polymerase Polδ. In hPolζ, hRev3 was shown to bind two copies of human Rev7 (hRev7) *via* adjacent Rev7-binding motifs (RBMs), RBM1 and RBM2, with the consensus sequence Pxxx(A/P)P (where 'x' is any residue) (29–32), while the consensus sequence of RBMs within ∼250 amino acid scRev7-interacting region of scRev3 is yet to be established (10, 20, 27, 33). Recent high-resolution cryo-EM structures of the scRev3:Rev7:Pol31:Pol32 assembly confirmed that scPolζ comprises two copies of scRev7 and narrowed the location of the two adjacent scRev3-RBMs (34, 35) (Fig. 1).

Rev7 is the master interaction module of Polζ that binds Rev3 and the TLS scaffold protein, the Y-family DNA polymerase Rev1, serving as a bridge between the extender and inserter polymerases in Rev1/Polζ-dependent TLS (36–38). Rev7 belongs to the HORMA (Hop1, Rev7, Mad2) family of adaptor proteins (39), which mediate two important types of protein–protein interactions: (i) binding peptide motifs of their partners underneath the safety-belt loop region and (ii) homodimerization and heterodimerization with HORMA proteins *via* a conserved interface (29–32, 39–43). Thus, hRev7 binds RBMs of hRev3 and other proteins by a mechanism wherein the C-terminal region of hRev7 entraps a peptide

* For correspondence: Dmitry M. Korzhnev, korzhniev@uchc.edu.

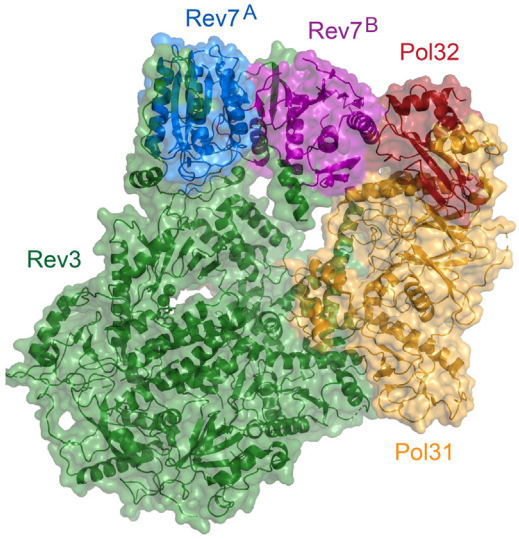

Figure 1. The cryo-EM structure of the five-subunit scPolζ assembly (PDB: 6V93). scPolζ, *S. cerevisiae* Polζ.

between the safety-belt loop and the core of hRev7 (29, 32, 40–47). In addition, hRev7 (alone or bound to an hRev3-RBM peptide) forms a symmetric head-to-head homodimer in solution, which can be disrupted by single point mutations, as well as heterodimerizes with HORMA family members, Mad2 and p31^{comet}, *via* the canonical dimerization interface (29, 31, 32). hRev7 also forms a compact dimer in the context of the 2:1 complex with a longer hRev3 fragment encompassing both RBMs (hRev3-RBM12), which mimics hRev7 behavior within the hPolζ assembly (29). Furthermore, structural studies of hRev7 bound to the two RBMs of the SHLD3 subunit of the shieldin complex, which suppresses DNA end resection during nonhomologous end joining (48–52), revealed a head-to-head dimer of the hRev7 protomers in open and closed conformations mediated by the same conserved HORMA interface (47).

Although *S. cerevisiae* has long served as the model system for studying TLS, the lack of information on structure and stoichiometry of scPolζ subunits obscured understanding of scPolζ assembly and regulation. A breakthrough study of the scPolζ architecture reported a stoichiometric complex of scRev3:scRev7:Pol31:Pol32 subunits at 1:1:1:1 ratio (21), and the initial low-resolution electron microscopy (EM) structure of the four-subunit complex was modeled with one copy of scRev7 (20), posing the question whether the Rev7 dimerization is a distinct property of the Polζ assembly in higher eukaryotes. Recently, three high-resolution cryo-EM structures of scPolζ were reported (PDB: 6V8P, 6V93, 7LXD), a remarkable feat that describes the spatial organization of scPolζ subunits and a variety of protein interactions within the scPolζ complex (34, 35) (Fig. 1). The structures reveal the scRev7:scRev3 interaction in a 2:1 stoichiometry, with the two scRev7 protomers forming an asymmetric head-to-tail dimer with a much smaller interface than the symmetric head-to-head hRev7 dimer or other dimers formed by HORMA protein pairs (34, 35). The unexpected mode of scRev7 dimerization observed in the high-resolution cryo-EM structures of scPolζ (34, 35) and conflicting earlier reports on scPolζ stoichiometry (20, 21) highlight the potential differences in Polζ structural arrangements in higher and lower eukaryotes that warrant further investigation.

Previous biochemical and structural studies of scPolζ lacked complementary biophysical data to aid the explanation of the scRev7:scRev3 assembly mechanism. We sought to elucidate the assembly of the scRev7:scRev3 complex using a combination of biophysical techniques to gain insights into the evolution of protein–protein interactions within eukaryotic Polζ. This work is aimed to determine the consensus scRev3-RBMs and validate their interactions with scRev7, confirm the 2:1 stoichiometry of the scRev7:Rev3 complex, and investigate the scRev3-mediated scRev7 dimerization in solution. While we have validated the two adjacent RBMs within scRev3, our studies have not confirmed the novel head-to-tail dimerization of scRev7 observed in the recent cryo-EM structures of scPolζ (34, 35), instead suggesting that scRev7 lacks the ability to form dimers in solution either alone or when tethered by scRev3-RBMs, which is a property that may have emerged later in evolution.

Results

Mapping RBMs in scRev3

Tentative scRev7-binding site(s) of scRev3 were previously mapped to a region encompassing residues 362 to 644 located between the predicted N-terminal domain and the inactive exonuclease domain (10, 20, 27, 33). We sought to determine the consensus sequence and validate RBMs within this region of scRev3 using bioinformatic analysis. Secondary structure prediction with Jpred (53) identified two sequences within this region with a pair of prolines (P526,P527 and P610,P611) preceded by a β-sheet and followed by an α-helix (Fig. 2*A*), matching the secondary structure adapted by hRev3-RBMs in complex with hRev7 (29, 32). Alignment of these two tentative RBM regions within Rev3 (below termed as RBM1 and RBM2) across the budding yeast subphylum (54) (Fig. S1, summarized in Fig. 2*B*) revealed a consensus yeast Rev3-RBM, ΦψyxxpPnyxxΦxxΦΦ, where Φ is hydrophobic aromatic or bulky aliphatic residue (W,F,Y,I,L,V), ψ is hydrophobic or polar/charged residue with a long aliphatic side-chain (I,L,V,M,R,K,E,Q), 'n' is helix-capping residue (N,D,S,T,C,G) (55), 'y' is tyrosine, phenylalanine or other residue, 'p' is proline or other residue, 'x' is any residue, and '-' is blank or any residue. The N-terminal portion Φψyxx-pP is better conserved in yeast Rev3-RBM2 with a strong preference for W in the first position and an invariable second proline of the pP pair, while the prolines may be substituted by other residues in yeast Rev3-RBM1. The C-terminal sequence of yeast Rev3-RBMs, nyxxΦxxΦΦ, is characteristic of an amphipathic α-helix starting with an N-capping residue 'n' with hydrophobic 'y' and 'Φ' residues clustered on one side of the helix. This part of yeast Rev3-RBMs is more variable with the last two hydrophobic residues or the entire sequence missing for some species (Figs. 2*B* and S1), which is consistent with a lack of C-terminal α-helix in the structures of several human RBMs (CAMP, SHLD2) bound to hRev7 (44–47). The consensus yeast Rev3-RBM aligns well with RBMs from hRev3 (29–32) and other human proteins (44–47) (Fig. 2*C*) except that the first and second 'y' (Y, F, or other residue)

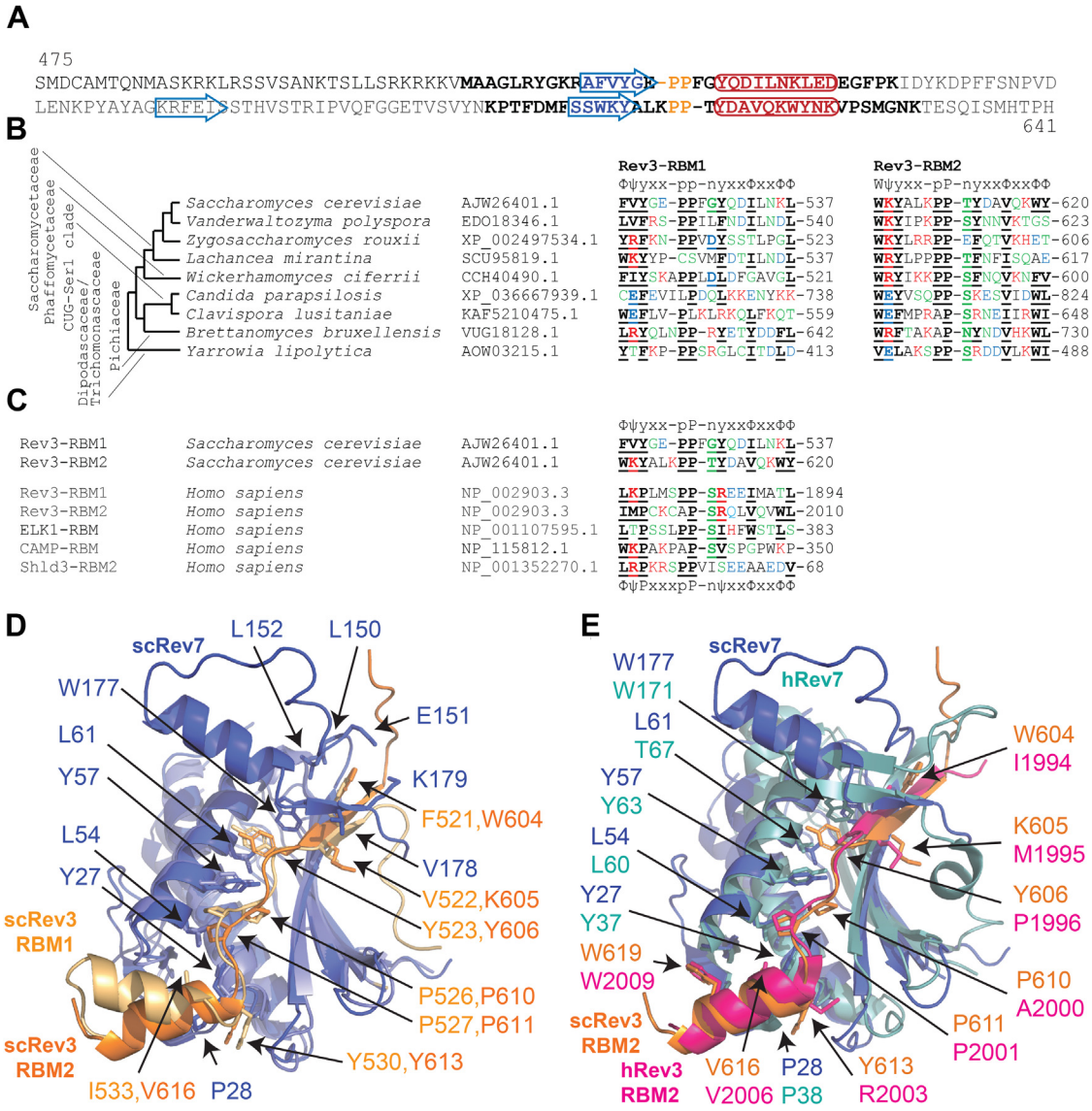

Figure 2. ScRev7 is predicted to have two Rev7 binding motifs (RBMs). *A*, secondary structure prediction of the Rev7 binding region within scRev3 with β-sheets and α-helices shown by *blue arrows* and *red rectangles*, respectively. *Bolded* are scRev3 regions 510 to 544 and 595 to 629 predicted to bind scRev7 characterized in this work. *B*, sequence alignments of the predicted Rev3-RBMs across the budding yeast subphylum with the phylogenic tree including classification into major clades shown on the left. Residues highlighted in *green* are polar (S,T,Q,N,C,G), in *red* are positively charged (R,K,H), in *blue* are negatively charged (*D* and *E*), and in *black* are hydrophobic (A,V,I,L,M,F,Y,W,P). Consensus sequences of yeast Rev3 RBM1 and RBM2 are shown on the top (see text for details). *C*, sequence alignment of scRev3-RBM1 and scRev3-RBM2 with various *H. sapiens* RBMs with consensus sequences for yeast (*top*) and human (*bottom*) RBMs. *D* and *E*, structural alignments of (*D*) scRev7/scRev3-RBM1 (*light blue/yellow*) and scRev7/scRev3-RBM2 (*blue/orange*) derived from the cryo-EM structure of scPolζ (PDB: 6V93) and (*E*) yeast scRev7/scRev3-RBM2 (*blue/orange*; PDB: 6V93) and human hRev7/hRev3-RBM2 (*cyan/pink*; PDB: 6BC8) complexes, which confirm sequence alignments in (*B* and *C*). Key residues involved in Rev7/Rev3-RBM interaction are highlighted. hRev7, Human Rev7; scPolζ, *S. cerevisiae* Polζ.

in yeast Rev3-RBM are substituted, respectively, with P and ψ in human Rev3-RBM. Thus, RBM can be generally defined as Φψ(y/P)xx-pP-n(y/ψ)xxΦxxΦΦ, where the first/second symbol in brackets corresponds to yeast/human proteins. Based on secondary structure prediction (Fig. 2*A*) and sequence conservation (Figs. 2, *B* and *C* and S1), we hypothesize the scRev3 regions 510 to 544 (RBM1) and 595 to 629 (RBM2) to bind scRev7.

To corroborate sequence alignments of yeast Rev3-RBM regions (Fig. 2, *A*–*C*), we superimposed coordinates of the scRev7^{A}/scRev3-RBM1 and scRev7^{B}/scRev3-RBM2 modules extracted from the cryo-EM structure of scPolζ (PDB: 6V93) (Fig. 2*D*). Despite a shorter scRev3-RBM1 β-sheet and a missing density in the scRev7^{A} safety-belt region, the structures of scRev3-RBM1 and scRev3-RBM2 fragments superimposed well, revealing nearly identical arrangement of the conserved RBM residues (except the C-terminal residues of an RBM α-helix) in agreement with sequence alignment (Fig. 2, *A*–*C*). Furthermore, superposition of scRev7^{B}/scRev3-RBM2 with the structure of human hRev7/hRev3-RBM2 complex (PDB: 6BC8) revealed a precise match in positions of all key RBM residues that interact with a conserved set of residues in Rev7 (Fig. 2*E*). Overall, sequence and structural alignments of yeast and human Rev3-RBM regions (Fig. 2) point to a high conservation of the Rev7:Rev3-RBM interaction.

Two scRev3-RBMs bind scRev7 with significantly different affinities

Next, we aimed to validate scRev7 binding to the two tentative scRev3-RBMs using a combination of biochemical techniques. His-tagged scRev7 co-expressed with RBM1 or RBM2 peptides and purified *via* cobalt affinity and size-exclusion chromatography (SEC) exhibited higher purification yields than apo-scRev7 (Fig. 3*A*), providing initial evidence that scRev3-RBMs can bind and stabilize the scRev7 protein. Bands correlating to the size of scRev7 and scRev3-RBM

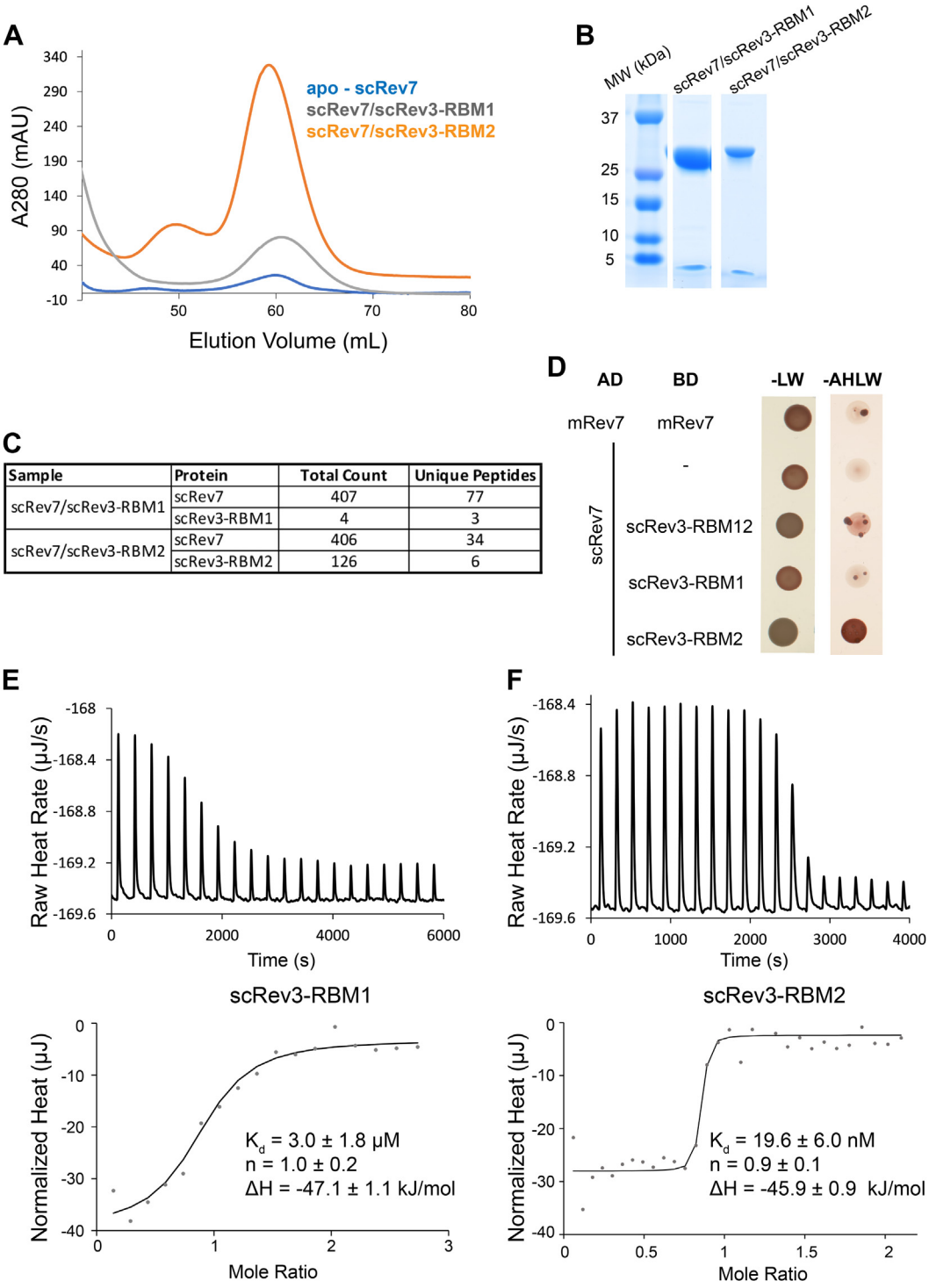

Sample	Protein	Total Count	Unique Peptides
scRev7/scRev3-RBM1	scRev7	407	77
	scRev3-RBM1	4	3
scRev7/scRev3-RBM2	scRev7	406	34
	scRev3-RBM2	126	6

Figure 3. ScRev3-RBM1 and scRev3-RBM2 are confirmed as scRev7 binding motifs. *A*, SEC chromatogram of apo-scRev7, and scRev7 co-expressed with either scRev3-RBM1 or scRev3-RBM2. *B*, SDS-page gels of scRev7/scRev3-RBM1 and scRev7/scRev3-RBM2 purified by affinity, size-exclusion, and ion-exchange chromatography. *C*, ScRev7 and RBM peptides detected in LC/MS-MS analysis of purified scRev7/scRev3-RBM1 and scRev7/scRev3-RBM2 samples. *D*, Y2H analysis of scRev7-AD and scRev3-BD interactions. *E* and *F*, isothermal titration calorimetry (ITC) thermograms of scRev3-RBM1 and scRev3-RBM2 titrated into MBP-scRev7. AD, activation domain; -AHLW, plates lacking adenine, histidine, leucine, and tryptophan; BD, binding domain; MBP-scRev7, scRev7 fused to the maltose binding protein; RBM, Rev7-binding motif; SAXS, small-angle X-ray scattering; SEC, size-exclusion chromatography; Y2H, yeast 2-hybrid.

peptides are visible on SDS-PAGE gels of the resulting samples, suggesting the scRev3 fragments copurify alongside scRev7 in stable complex (Fig. 3*B*). Finally, mass spectrometry analysis confirmed the presence of scRev3-RBMs peptides in the purification samples (Fig. 3*C* and Table S2), suggesting the predicted RBMs bind scRev7.

We also validated scRev7 interaction with each of the two scRev3-RBMs, as well as with a longer scRev3 construct containing both RBMs (Rev3-RBM12, residues 510–629) *via* yeast 2-hybrid (Y2H) assays using scRev7 and scRev3 fragments fused with the activation domain (AD) and the DNA-binding domain (BD) of the *GAL4* transcription factor (56). Dimerization of AD- and BD-fused wildtype mouse Rev7 (mRev7) was used as a positive control (29). As expected, yeast grew on plates lacking adenine, histidine, leucine, and tryptophan (-AHLW plates) when transformed with scRev7-AD and scRev3-RBM1-BD, scRev3-RBM2-BD, or scRev3-RBM12-BD, suggesting scRev7 binds to the predicted scRev3-RBMs (Fig. 3*D*). A less robust growth of yeast transformed with the scRev7-AD:scRev3-RBM1-BD pair likely points to a weaker interaction. Y2H assays conducted in the reciprocal orientation using scRev7-BD and scRev3-RBM2-AD, or scRev3-RBM12-AD yielded similar results (Fig. S2).

Having confirmed scRev7 interaction with scRev3-RBM1 and scRev3-RBM2, we sought to quantify the binding affinities of scRev7 fused to the maltose binding protein (MBP-scRev7) for the individual RBM peptides using isothermal titration calorimetry (ITC). The data analysis suggests that scRev7 forms 1:1 complexes with each of the two scRev3-RBMs exhibiting similar binding enthalpies, yet significantly different affinities (Fig. 3, *E* and *F*). Thus, scRev7 binds scRev3-RBM2 with K_d of 19.6 ± 6.0 nM, which is over two orders of magnitude stronger than K_d of 3.0 ± 1.8 μM for scRev7:-scRev3-RBM1 interaction. These data are consistent with higher purification yields for scRev7 co-expressed with scRev3-RBM2 (Fig. 3*A*), higher counts of scRev3-RBM2 than scRev3-RBM1 peptides detected by mass spectrometry (Fig. 3*C*), weaker growth of scRev7-AD and scRev3-RBM1-BD transformants on -AHLW plates in Y2H assays (Fig. 3*D*) and higher conservation of scRev3-RBM2 among yeast species (Figs. 2*B* and S1). Collectively, our data validate RBM1 (residues 510–544) and RBM2 (residues 595–629) as the two scRev7-binding regions in scRev3 with scRev3-RBM2 being consistently the stronger binding partner.

scRev7 is a monomer in solution

Previous studies demonstrated that hRev7, alone or in complex with individual hRev3-RBMs, forms a homodimer in solution with K_d of 1.9 μM obtained by dilution ITC (29, 31, 32). In the context of hPolζ, the two copies of hRev7 bind to the two adjacent hRev3-RBMs facilitating the formation of a compact dimer, which is important for hPolζ function in TLS (29). To test whether scRev7 can homodimerize on its own like its human counterpart, we investigated oligomerization of the scRev7/scRev3-RBM2 construct using analytical ultracentrifugation (AUC) and small-angle X-ray scattering (SAXS) (Fig. 4). AUC analysis performed at protein concentrations ranging from 6 to 25 μM revealed a single sedimented species at ∼2.6S, corresponding to ∼32 kDa, with no evidence of dimerization equilibrium (Fig. 4*A*). The radius of gyration (R_g ∼ 24 Å) and molecular weight (MW ∼ 34 kDa) values derived from SAXS data were independent of protein concentration in the range of 65 to 260 μM and consistent with the predicted MW of 34.4 kDa for the scRev7/Rev3-RBM2 monomer (Fig. 4*B*). We also attempted dilution ITC measurements for scRev7 fused with scRev3-RBM2 by a 9xGS linker, which results in increased protein solubility. However, even with a syringe protein concentration of 450 μM, no heat release was detected that would be consistent with dimerization (Fig. S3). Furthermore, apo-scRev7, scRev7/scRev3-RBM1, and scRev7/scRev3-RBM2 elute at similar volumes during SEC purification (Fig. 3*A*), suggesting that oligomeric state of scRev7 is not affected by RBM binding. Collectively, these data show that scRev7 is a monomer in solution at concentrations up to ∼0.5 mM, which is a remarkable difference from dimerization behavior of the hRev7 protein (29, 31, 32). These data, however, cannot exclude a possibility that scRev7 may dimerize with weaker binding affinity than can be detected in our experiments (mM range) but nevertheless may form a stable dimer when the two copies of scRev7 are tethered together by scRev3-RBMs in the context of scPolζ.

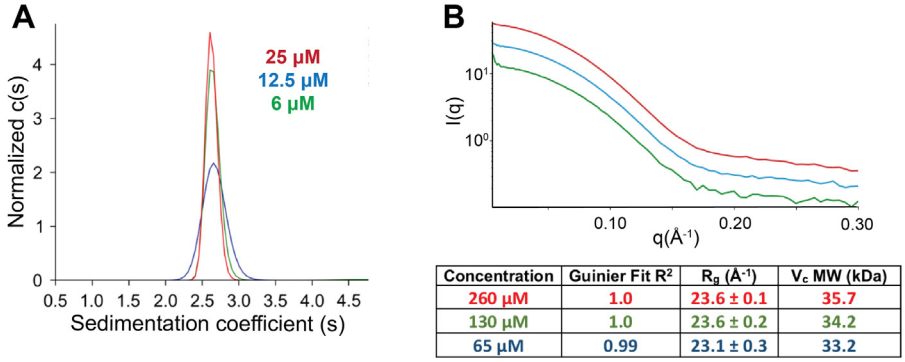

Concentration	Guinier Fit R^2	R_g (Å^{-1})	V_c MW (kDa)
260 μM	1.0	23.6 ± 0.1	35.7
130 μM	1.0	23.6 ± 0.2	34.2
65 μM	0.99	23.1 ± 0.3	33.2

Figure 4. ScRev7 is a monomer in solution. *A*, sedimentation velocity c(s) distribution analysis of scRev7 at three concentrations. *B*, SAXS scattering profiles with extracted parameters for scRev7/scRev3-RBM2 measured at different protein concentrations. RBM, Rev7-binding motif; SAXS, small-angle X-ray scattering.

scRev7 binds scRev3 in 2:1 stoichiometry

Next, we explored the stoichiometry and dimerization behavior of scRev7 when bound to the scRev3-RBM12 fragment encompassing residues 510 to 629, which includes both Rev7-binding RBM1 and RBM2 regions that are separated by ∼50 amino acids. To confirm this scRev3 fragment can bind two copies of scRev7 at the same time, scRev7 was co-expressed with scRev3-RBM12, and stoichiometry of the complex was examined by SEC, AUC, and SAXS. During SEC purification on a Superdex 75 column (GE Healthcare), scRev7/scRev3-RBM12 elutes ∼10 ml earlier than scRev7/scRev3-RBM2 consistent with doubling molecular weight of the complex (Fig. 5*A*). Sedimentation velocity AUC analysis corroborate with the SEC results, wherein scRev7/scRev3-RBM12 and scRev7/scRev3-RBM2 exhibit sedimentation coefficients (S-values) of 4.1S and 2.6S in agreement with a 2:1 and 1:1 scRev7/scRev3 binding stoichiometry, respectively (Fig. 5*B*). SAXS data agree with the SEC and AUC results, revealing a MW of ∼83 kDa for scRev7/scRev3-RBM12 consistent with the predicted MW for the 2:1 complex (76.1 kDa) (Fig. 5*C*). Taken together, the SEC, AUC, and SAXS data corroborate a 2:1 stoichiometry of scRev7:scRev3-RBM12 interaction in solution.

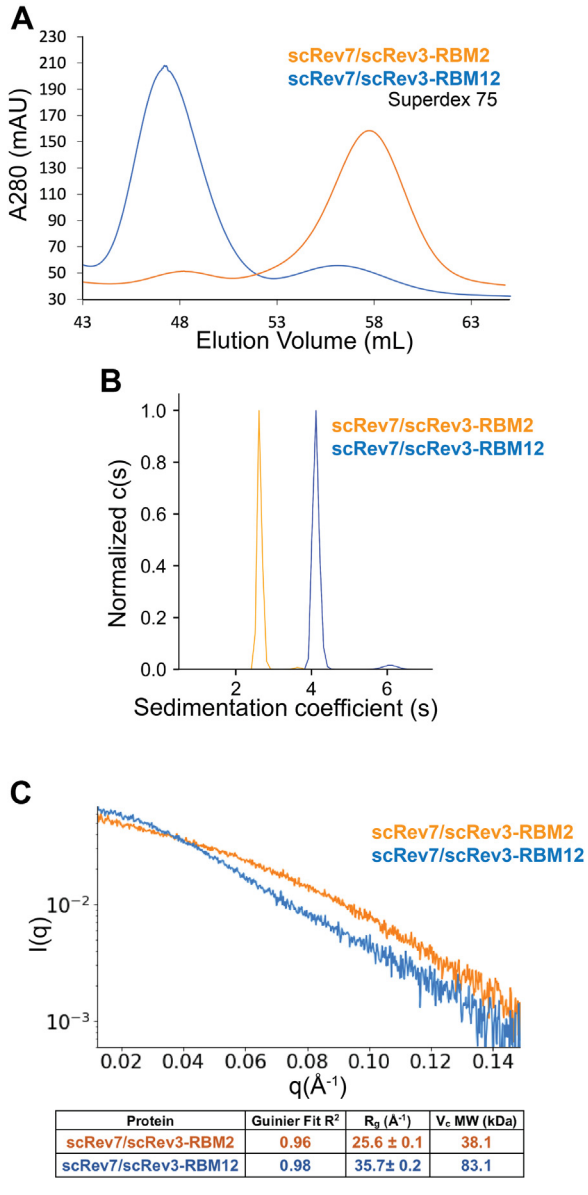

Protein	Guinier Fit R^2	R_g (Å^{-1})	V_c MW (kDa)
scRev7/scRev3-RBM2	0.96	25.6 ± 0.1	38.1
scRev7/scRev3-RBM12	0.98	35.7± 0.2	83.1

Figure 5. ScRev7/scRev3-RBM12 has a 2:1 stoichiometry. *A–C*, (*A*) SEC profiles, (*B*) sedimentation velocity c(s) distribution analysis (18 μM scRev7 protomer concentration), and (*C*) SAXS scattering profiles (53 μM scRev7 protomer concentration) with extracted parameters for scRev7/scRev3-RBM2 and scRev7/scRev3-RBM12. RBM, Rev7-binding motif; SEC, size-exclusion chromatography; SAXS, small-angle X-ray scattering.

Mutating dimer interface does not affect shape of the scRev7/scRev3-RBM12 complex

Although scRev7 binds scRev3 in a 2:1 stoichiometry, we found that scRev7 on its own is a monomer and have yet to obtain any data suggesting that scRev7 can homodimerize in solution when bound to scRev3-RBM12. Recent high-resolution cryo-EM structures corroborate a 2:1 scRev7:-scRev3 stoichiometry within scPolζ with each scRev7 protomer binding to scRev3-RBM1 and scRev3-RBM2 regions (34, 35). In contrast to hRev7, which forms symmetric head-to-head dimer through the canonical HORMA interface centered around helix αC (29, 47), the cryo-EM structures (PDB: 6V8P, 6V93, 7LXD) suggest that scRev7 dimerizes asymmetrically in a head-to-tail fashion (Fig. 6*A*) (34, 35). The scRev7 dimer interface in the cryo-EM structures has an average buried surface area of ∼500 Å^2 per protomer, which is significantly smaller than the hRev7 dimer interface of 828 Å^2 and 755 Å^2 per monomer in the crystal structure of shieldin assembly (PDB: 6KTO) (47) and a docked model of hRev7/hRev3-RBM2 homodimer (PDB: PDBDEV_00000009) (29), respectively.

Our strategy to probe scRev7 dimerization when bound to scRev3 was to design potential dimer-breaking mutations guided by cryo-EM structures of scPolζ (34, 35) and study solution behavior of scRev7/scRev3-RBM12 variants using a combination of biophysical techniques. Analysis of the scRev7 dimer interface using PISA software (57) reveals five hydrogen bonds and a salt bridge that facilitate scRev7 dimerization (Fig. 6*B*). Residues that mediate these interactions were mutated, including N41, D115, R118, and S119 of the first scRev7 protomer that align with the canonical HORMA interface on or near helix αC (29, 31, 32) and H154, D157, K175, and K179 on the opposite face of the second scRev7 protomer (Fig. 6*B*). All considered scRev7/scRev3-RBM12 variants elute at similar volumes as the WT construct during SEC, indicating the mutations did not disrupt the 2:1 stoichiometry of the complex (Fig. 6*C*). AUC analysis corroborates with the SEC data with all scRev7/scRev3-RBM12 mutants sharing a similar S-value with the WT construct, suggesting no change to the 2:1 stoichiometry (Fig. 6*D*). This is an expected result, since K_d of scRev7 for scRev3-RBM1 and scRev3-RBM2 are 3.0 μM and 19.6 nM, respectively, and AUC experiments for scRev7/scRev3-RBM12 variants were conducted at 12.5 μM scRev7 monomer concentration.

Although the scRev7/scRev3-RBM12 variants retain 2:1 stoichiometry, interface mutations may be sufficient to break the scRev7 dimer and change protein shape as monitored by SAXS experiments. If scRev7 forms a compact dimer when bound to scRev3-RBM12, then the dimer-breaking mutations should elongate and increase flexibility of the complex, a

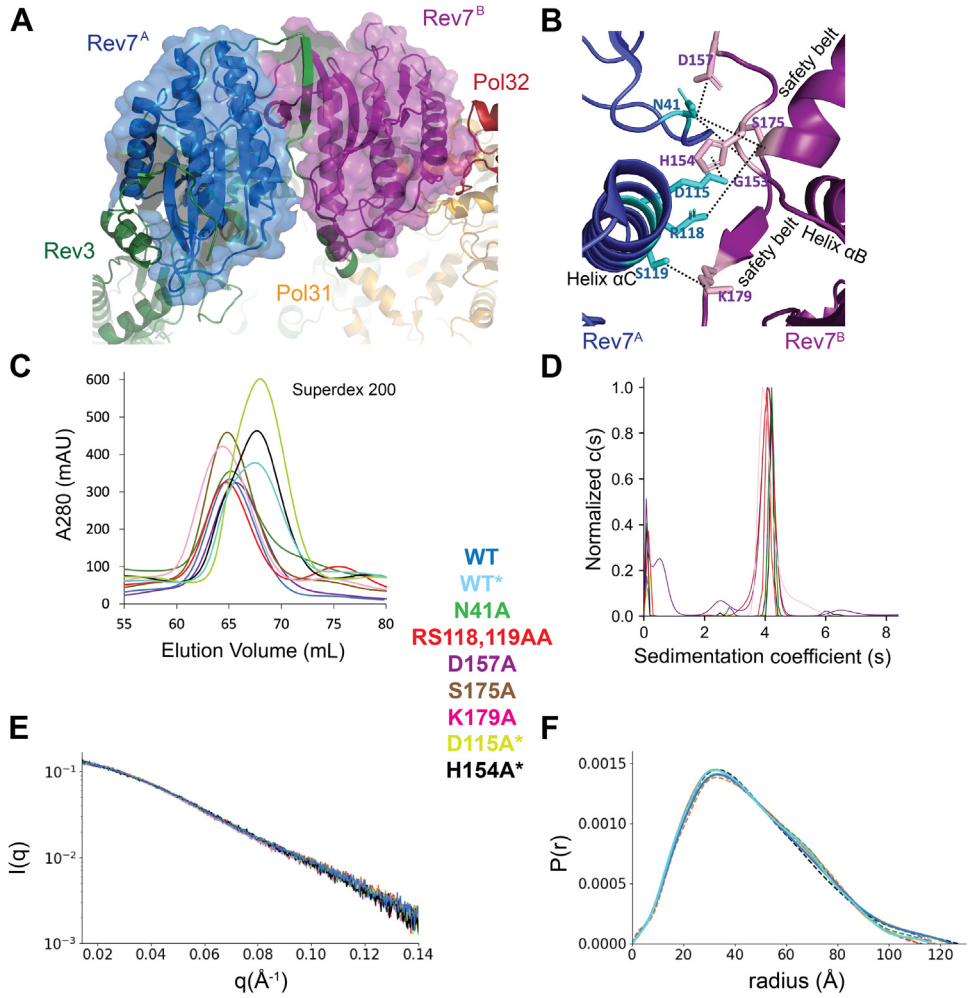

Figure 6. Mutagenesis of the dimer interface does not affect 2:1 stoichiometry or shape of the scRev7/scRev3-RBM12 complex in solution. *A*, an asymmetric head-to-tail scRev7 dimer in the context of the cryo-EM structure of scPolζ (PDB: 6V93). *B*, close up view of the scRev7 dimer interface within the cryo-EM structure. *C* and *D*, (*C*) SEC profiles of scRev7/scRev3-RBM12 WT and dimer interface mutants (mutants in a second batch purified on a different column are marked with *asterisk*), (*D*) sedimentation velocity c(s) distribution analysis for the dimer interface mutants (12.5 μM Rev7 protomer concentration). *E* and *F*, (*E*) SAXS scattering profiles and (*F*) P(r) pair distance distributions for scRev7/scRev3-RBM12 dimer interface mutants (53 μM Rev7 protomer concentration). RBM, Rev7-binding motif; SEC, size-exclusion chromatography; SAXS, small-angle X-ray scattering; scPolζ, *S. cerevisiae* Polζ.

phenomenon observed in the SAXS studies of hRev7 dimer-breaking mutants (29). The SAXS profiles measured for WT and mutant scRev7/scRev3-RBM12 were similar, indicating no significant change in either size or shape of the protein complex (53 μM samples Fig. 6*E*; 26 μM samples Fig. S4*A*). The pair distance distributions P(r) calculated from SAXS profiles were comparable for all scRev7/scRev3-RBM12 variants with the maximum dimension D_{max} of ∼120 Å, suggesting no elongation caused by mutations of the cryo-EM dimer interface (Figs. 6*F* and S4*B*). Thus, contrary to our expectations, matching SAXS profiles and P(r) distributions for WT and mutant scRev7/scRev3-RBM12 suggest that neither the HORMA nor asymmetric scRev7 dimer interface mutations affect the shape of 2:1 scRev7/scRev3-RBM12 complex.

scRev7/scRev3-RBM12 complex is elongated and flexible in solution

To elucidate whether WT scRev7/scRev3-RBM12 adopts a compact conformation in solution consistent with scRev7 dimerization (34, 35), we compared experimental SAXS data with theoretical profiles generated by Crysol (58) for the 2:1 scRev7/scRev3-RBM12 module as it appears in the cryo-EM structure of scPolζ (34, 35). Protein flexibility was assessed *via* Kratky analysis, wherein globular proteins with minimal flexibility exhibit a Gaussian peak of $I(q)q^2$ *versus* q that depreciates to zero at high q, while flexible proteins display an asymmetric peak that slowly depreciates and plateaus above zero (59). As a control, we extracted coordinates of the 1:1 scRev7/scRev3-RBM2 module from the cryo-EM structure of scPolζ and generated theoretical SAXS profiles for this complex for the comparison with experimental data (Fig. 7, *A*–*C*). The theoretical SAXS curve and P(r) distribution for scRev7/scRev3-RBM2 overlayed well with the experimental data (Fig. 7, *A* and *B*) in agreement with a single conformation of this module as observed by cryo-EM. The Kratky analysis also revealed matching experimental and theoretical curves with Gaussian peaks suggestive of a rigid conformation of the scRev7/scRev3-RBM2 monomer in solution (Fig. 7*C*). Taken together, P(r) and Kratky analyses confirm that the cryo-EM

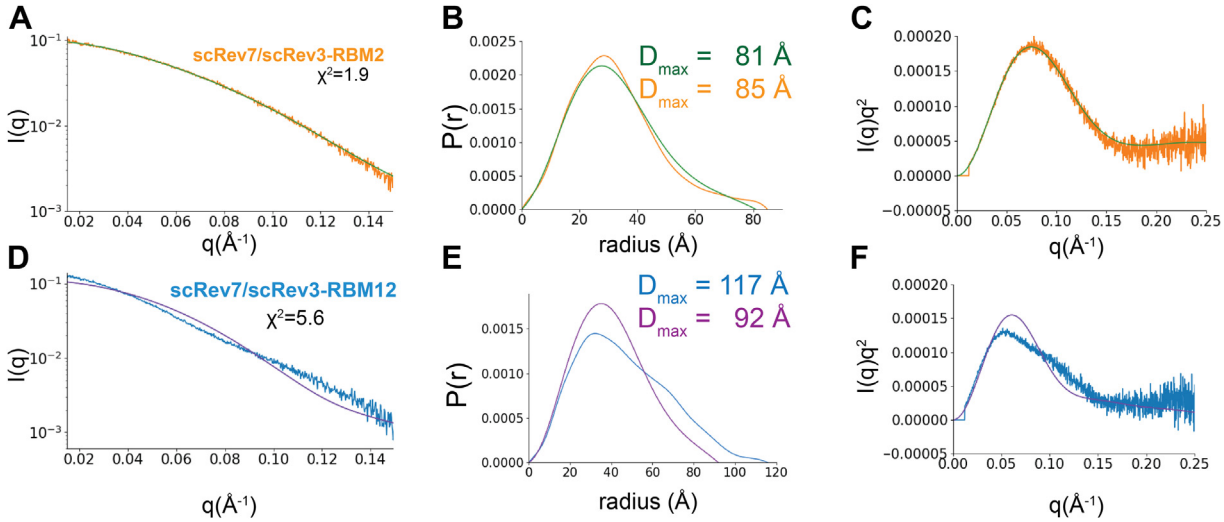

Figure 7. ScRev7 does not dimerize within the scRev7/scRev3-RBM12 complex. *A–C*, experimental (*orange*) and theoretical (*green*) SAXS profiles (*A*), P(r) distributions (*B*), and Kratky plots (*C*) for scRev7/scRev3-RBM2. *D–F*, experimental (*blue*) and theoretical (*violet*) SAXS profiles (*D*), P(r) distributions (*E*), and Kratky plots for scRev7/scRev3-RBM12 (*F*). RBM, Rev7-binding motif; SAXS, small-angle X-ray scattering.

conformation of scRev7/scRev3-RBM2 accurately reproduces the experimental SAXS data.

In contrast, the theoretical SAXS profile for the 2:1 scRev7/scRev3-RBM12 complex aligns poorly with the experimental data (Fig. 7*D*), and the P(r) analysis reveals this complex is significantly elongated in solution relative to the cryo-EM structure, as suggested by ∼25 Å difference in experimental and theoretical D_{max} (Fig. 7*E*). Kratky analysis of the experimental data displays an asymmetric peak that depreciates slower than the theoretical data, indicating scRev7/scRev3-RBM12 is more flexible in solution than expected from the cryo-EM structure (Fig. 7*F*). Overall, SAXS data for scRev7/scRev3-RBM12 are inconsistent with the rigid asymmetric head-to-tail dimer of scRev7 observed in the cryo-EM structure of scPolζ (34, 35). Instead, the data suggest the two copies of scRev7 bound to scRev3-RBM12 behave as two beads connected by a flexible linker that diffuse freely relative to one another, explaining why the potential dimer breaking mutations have no effect on shape of the complex.

scRev7:scRev3-RBM12 interaction is solely driven by scRev3-RBM motifs

The cryo-EM structure of scPolζ suggests that a linker region connecting the two scRev3-RBMs (residues 545–594) might contribute to scRev7/scRev3 binding (34, 35). Specifically, residues 573 to 594 of scRev3 preceding RBM2 form contacts with αB and αC helices of the scRev7^{A} protomer and the safety belt region of scRev7^{B} (Fig. 8*A*), acting like a zipper that brings the two Rev7 protomers together. The zipper region is preceded by a loop region (residues 545–572) that makes contacts with the scRev3 catalytic domain. Considering moderate amino acid conservation in this scRev3-zipper region among yeast species (Fig. S5*A*) and its extensive interface with the scRev7 dimer in the cryo-EM structure of scPolζ (Fig. S5*B*), we sought to probe MBP-scRev7 interaction with scRev3-zipper by ITC. Unlike scRev3-RBM peptides (Fig. 3, *E* and *F*), the ITC thermograms for MBP-scRev7 titrated with the scRev3-zipper peptide display no heat release that would be consistent with binding (Fig. S5*C*), indicating that scRev3-zipper alone is unable to promote interaction between scRev7 protomers.

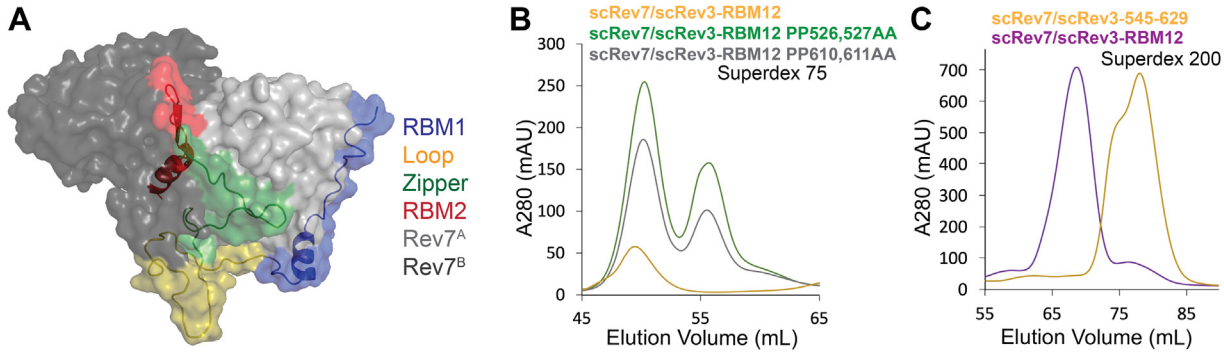

Figure 8. ScRev3-RBMs are solely responsible for scRev7/scRev3 2:1 stoichiometry. *A*, ScRev7/scRev3-RBM12 module from the cryo-EM structure of scPolζ (PDB: 6V93). *B*, SEC profiles for scRev7/scRev3-RBM12 WT, PP526,527AA, and PP610,611AA. *C*, SEC profiles of scRev7/scRev3-RBM12 and truncated scRev7/scRev3-545-629 lacking RBM1. RBM, Rev7-binding motif; scPolζ, *S. cerevisiae* Polζ; SEC, size-exclusion chromatography.

To further illustrate that scRev3-RBMs are the sole drivers of 2:1 stoichiometry of the scRev7:scRev3-RBM12 complex, we mutated pairs of proline residues in each of the scRev3 RBM1 and RBM2 regions and tested the complex formation by SEC. Both PP525,526AA and PP610,611AA mutants elute as a mixture of 2:1 and 1:1 species indicative of partial disruption of the scRev7/scRev3-RBM12 complex (Fig. 8*B*), revealing that prolines are essential but not the only mediators of binding. This observation agrees with Y2H assays, in which proline mutations in scRev3-RBM2 decreased but did not eliminate growth of scRev7-AD/scRev3-RBM2-BD transformants on -AHLW plates, suggesting other RBM2 residues contribute to interaction (Fig. S6). Furthermore, scRev7 co-expressed with the scRev3 peptide comprising the loop, zipper, and RBM2, but not RBM1 regions (residues 545–629), elutes as a 1:1 complex during SEC purification (Fig. 8*C*) demonstrating that scRev3-RBMs, but not the zipper region, promote scRev7/scRev3-RBM12 assembly in 2:1 stoichiometry.

Discussion

Polζ is a master extender polymerase in the two-step Rev1/Polζ-dependent TLS (4–6), which is composed of the core subunits, Rev3 and Rev7 (27, 28), and the two additional subunits, PolD2:PolD3 in humans (24, 25) and Pol31:Pol32 in yeast (21). Rev7 is a central scaffolding module of Polζ that binds Rev3 and mediates its recruitment to sites of DNA damage *via* interaction with Rev1 (36–38). In this study, we mapped the two RBMs in *S. cerevisiae* scRev3 encompassing residues 510 to 544 (RBM1) and 595 to 629 (RBM2) sharing a consensus sequence ΦψyxxpPnyxxΦxxΦΦ (where Φ is hydrophobic aromatic or bulky aliphatic residue, ψ is hydrophobic or polar/charged residue with a long aliphatic side-chain, 'n' is helix-capping residue (55), 'y' is Y, F or other residue, 'p' is P or other residue, 'x' is any residue, '-' is blank or any residue) (Fig. 2). We also confirmed scRev7 binding for both scRev3-RBMs by SEC co-purification combined with mass spectrometry analysis, Y2H assays, and ITC (Fig. 3). In agreement with higher sequence conservation in the RBM2 region, scRev7 binds scRev3-RBM2 two orders of magnitude stronger than scRev3-RBM1 (K_d of 19.6 nM *versus* 3.0 μM) (Fig. 3). Furthermore, we demonstrated that scRev7 forms a stable 2:1 complex with scRev3-RBM12 (residues 510–629), comprising both RBM1 and RBM2 regions (Fig. 5), suggesting that, like its human counterpart (29–32), scPolζ assembly includes two copies of scRev7.

Recent cryo-EM structures of scPolζ corroborated 2:1 stoichiometry of the scRev7:scRev3 interaction and confirmed our mapping of scRev3-RBMs (34, 35). Thus, the primary sequence alignment of yeast Rev3-RBMs (Figs. 2*B* and S1) agrees with structural superposition of the scRev7^{A}/scRev3-RBM1 and scRev7^{B}/scRev3-RBM2 modules (Fig. 2*D*), sequence alignment with human RBMs (Fig. 2*C*), and structural comparison of yeast and hRev7/Rev3-RBM2 complexes (Fig. 2*E*), pointing to conservation of the Rev7:Rev3-RBM interaction across species. The cryo-EM structures of scPolζ revealed that both scRev7 protomers adopt a closed conformation when bound to scRev3-RBMs whereby the ligand is locked underneath the safety-belt loop of scRev7. Consistent with a stronger binding affinity, scRev3-RBM2 in complex with scRev7^{B} forms the β-strand and the α-helix predicted by bioinformatic analysis (Fig. 2), whereas the β-strand predicted for scRev3-RBM1 bound to scRev7^{A} is shorter and scRev7^{A} is missing density is in the safety-belt region (34, 35). The more stable scRev7^{B}/scRev3-RBM2 module forms an extensive interface with Pol31:Pol32, highlighting the significance of scRev7 interactions with these accessory subunits.

The two hRev7 protomers form a head-to-head dimer *via* the canonical HORMA dimerization interface when bound to an isolated RBM (29, 31, 32) and when tethered together by fragments of hRev3 (29) or the SHLD3 subunit of shieldin (47) comprised of two RBM regions. The homodimer interface of hRev7, centered around helix αC, is also utilized for heterodimerization with other HORMA proteins, Mad2 and p31^{comet} (29). In a stark contrast to hRev7, the cryo-EM structures of scPolζ revealed an asymmetric head-to-tail dimerization of scRev7 through a much smaller interface never before observed among HORMA proteins (34, 35). In this study, we investigated dimerization behavior of scRev7 in solution using a combination of SEC, AUC, ITC, SAXS, and mutagenesis. To our surprise, scRev7 alone or in complex with individual scRev3-RBMs was monomeric in solution at protein concentrations up to ∼0.5 mM, suggesting that scRev7 lacks the intrinsic ability to homodimerize like its human counterpart (Figs. 3 and 4). Mutagenesis to the cryo-EM dimer and predicted HORMA dimer interfaces did not alter the size, shape, or stoichiometry of the 2:1 scRev7/scRev3-RBM12 complex (Fig. 6), suggesting these interfaces take no part in scRev7 dimerization within the tethered complex. Furthermore, SAXS data revealed that the 2:1 scRev7/scRev3-RBM12 complex is flexible and more elongated in solution than the head-to-tail scRev7 dimer linked by scRev3-RBM12 in the cryo-EM structures of scPolζ (34, 35) (Fig. 7), suggesting the tethered scRev7 protomers do not assemble into a compact dimer. We also demonstrated that the two scRev3-RBMs are the sole determinants of 2:1 stoichiometry of the scRev7/scRev3-RBM12 complex, while the linker region between RBMs (comprised of the loop and zipper regions) alone does not interact with scRev7 in solution despite extensive contacts it forms with both scRev7 protomers in the cryo-EM structures of scPolζ (Figs. 8 and S5). Taken together, our results indicate that scRev7 does not dimerize in solution either on its own accord or when bound to the scRev3-RBM12 fragment comprising the two RBMs, nor is scRev7 dimerization mediated by the liker region between scRev3-RBMs.

The likely reason for the discrepancy between the dynamic behavior of the 2:1 scRev7/scRev3-RBM12 module in solution and its rigid configuration in the cryo-EM structures of scPolζ (34, 35) is that the two scRev7 protomers may be locked in their positions within scPolζ by various interactions with other subunits. Thus, the cryo-EM structures revealed that the scRev7^{B} protomer interacts with both Pol31 and the N-terminal domain of Pol32, whereas the scRev3-loop region between scRev3-RBM1 and scRev3-zipper interacts with the

palm and thumb domains of the scRev3 catalytic core (Fig. 8). It is conceivable that interaction of the loop region with the scRev3 catalytic core causes scRev3-loop to adopt a hairpin structure, which shortens the distance between scRev3-RBMs and brings the scRev7 protomers together thus locking the scRev7 dimer and constraining the scRev3-zipper. Another possible explanation for the reported discrepancy is that the scRev7 dimer tethered by scRev3-RBM12 in the cryo-EM structure of scPolζ is only transiently sampled and sparsely populated in solution. This argument is supported by a smaller interface of the head-to-tail scRev7 dimer observed by cryo-EM (34, 35) than the interfaces of the canonical head-to-head hRev7 dimers (29, 47).

Protein interactions mediated by the Rev7 subunit of Polζ are essential for resistance to DNA damage in yeast and mammalian cells (27) Thus, both RBMs of mouse Rev3 were required to confer resistance to cisplatin- and UV-induced DNA damage in Rev3$^{-/-}$ mouse embryonic fibroblasts (30, 60). Furthermore, mRev7 mutants that are deficient in dimerization *via* the canonical HORMA interface were unable to restore viability of Rev7$^{-/-}$ cells after cisplatin treatment (29), suggesting that interactions mediated by this interface are important for DNA damage response. At least two DNA damage response pathways utilize homodimerization of hRev7 protomers tethered together by a protein with the two consecutive RBMs. Besides its dimerization within the TLS DNA polymerase hPolζ when tethered by hRev3-RBMs (29), hRev7 also forms a homodimer when bound to RBMs of the SHLD3 subunit of the shieldin complex, which mediates the choice of DNA double-strand break repair pathway (48–52). The same interface of hRev7 is utilized for its heterodimerization with p31^{comet} (29), a HORMA protein facilitating disassembly of hRev7 complexes with hPolζ and shieldin by the TRIP13 AAA+ ATPase and promoting hRev7 recycling (61–63). A loss of any of these hRev7 interactions would result in a DNA damage sensitive phenotype. Interestingly, the SHLD1, SHLD2, and SHLD3 subunits of the shieldin complex, which harbors the Rev7 homodimer, arose in vertebrates and are missing in *S. cerevisiae* (52). Here we demonstrated that scRev7, while forming the 2:1 complex with scRev3 mediated by RBMs, is devoid of homodimerization in solution. This represents an important difference in the Polζ assembly mechanism in yeast and humans, highlighting evolution of Rev7 interactions within eukaryotic Polζ. Whether scRev7 can heterodimerize *via* the canonical interface with other HORMA proteins remains to be investigated. It is possible that Rev7 homodimerization is a mechanism that emerged later in evolution with the expanding repertoire of Rev7 functions.

Experimental procedures

Secondary structure prediction, sequence, and structural alignments

Secondary structure was predicted using Jpred (53). Clustal Omega was used for multiple sequence alignments with manual modifications (64). Structural superposition of scRev7^{A}/scRev3-RBM1 with scRev7^{B}/scRev3-RBM2 (PDB: 6V93), and scRev7^{B}/scRev3-RBM2 with hRev7/hRev3-RBM2 (PDB: 6BC8) was performed in PyMOL (65).

Subcloning and mutagenesis

The pETDuet-1 (Novagen) plasmids for co-expression in *E. coli* of scRev7 and scRev3 fragments were generated using standard molecular biology techniques. The codon optimized genes encoding scRev7 and scRev3 fragments, including scRev3-RBM1 (residues 510–544), scRev3-RBM2 (residues 595–629), scRev3-RBM12 (residues 510–629), and a truncated scRev3 fragment containing RBM2, but not RBM1 (residues 545–629), were subcloned into the multiple cloning sites 1 and 2 (MCS-1 and MCS-2) of pETDuet-1, respectively. In the pETDuet-1 construct for overexpression of apo-scRev7, MCS-2 was empty. Mutations to the constructs were introduced using a standard PCR site-directed mutagenesis (66). To generate an overexpression construct for MBP-scRev7 fusion (used for ITC binding studies of scRev7 with scRev3 fragments), codon optimized scRev7 gene was subcloned into a pET28-MBP-TEV vector. In addition, DNA encoding scRev7 fused with scRev3-RBM2 by a 9xGS linker was subcloned into MCS-1 of pETDuet-1 vector with an empty MCS-2. For Y2H assays, DNA encoding scRev7, scRev3-RBM1, scRev3-RBM2, and scRev3-RBM12 were subcloned as fusions with *GAL4* AD and BD in pGAD-C1 and pGBD-C1 vectors, respectively, with mutations introduced using a standard PCR site-directed mutagenesis (66).

Protein expression and purification

Plasmids were transformed into *E. coli* BL21(DE3) cells, and bacterial culture was grown in LB medium (1L for comparative SEC) at 37 °C until reaching OD_{600} 0.8 to 1.0. Protein expression was induced by 1 mM isopropyl β-d-1-thiogalactopyranoside (IPTG) at 20 °C overnight. Cells were lysed by sonication in 20 mM $NaHPO_4$, 300 mM NaCl, and 10 mM imidazole, followed by protein purification using cobalt affinity chromatography and SEC with a Superdex 75 or 200 column (GE Healthcare). Apo-scRev7, scRev7/scRev3-RBM1, scRev7/scRev3-RBM2, scRev7/scRev3-RBM12, their mutational and truncational variants, and scRev7/scRev3-RBM2 9xGS fusion were eluted in a buffer containing 20 mM Tris, 100 mM NaCl, 2 mM EDTA, 1 mM DTT, pH 8, while MBP-scRev7 was eluted in the same buffer with pH 8.4 (resulting in 10–30 μM elution fraction concentration for proteins expressed in 1L of LB). Apo-scRev7, scRev7/scRev3-RBM1, scRev7/scRev3-RBM2, scRev7/scRev3-RBM12 and their variants were further purified by ion-exchange chromatography with a HiTrap Q HP column.

Mass spectrometry

Proteins were digested using Endoproteinase AspN with digestion quenched by concentrated formic acid. Peptides were desalted using Pierce C18 spin columns (P/N 89,870) and loaded onto a 25 cm nanoEase m/*z* BEH C18 analytical column (Waters Corporation) using a Thermo Scientific Ultimate 3000 RSLCnano UPLC instrument directly coupled to a Thermo Scientific Q Exactive HF mass spectrometer. Peptides

were separated *via* a reversed phase gradient 1 h in length with a 300 nl/min flow rate and directly eluted into the mass spectrometer using positive mode electrospray ionization through a New Objective PicoTip emitter. Peptides were mass analyzed using a Top15 data-dependent acquisition method; MS/MS spectra were generated using higher-energy C-trap dissociation. Peptide and protein identification and quantification was achieved using the Andromeda search engine and MaxQuant quantitative software (v1.6.0.1) (67). The raw data were searched against the full Uniprot *E. coli* reference proteome plus the recombinant scRev7, scRev3-RBM1, and scRev3-RBM2 primary sequences. Peptide and protein-level quantification was performed using the MaxLFQ algorithm.

Isothermal titration calorimetry

Measurements were performed on an Affinity ITC LV calorimeter (TA Instruments) at 25 °C. To probe scRev7 interactions with the two scRev3-RBMs and the linker region between RBMs, MBP-scRev7 and scRev3 peptides, including scRev3-RBM1 (residues 510–544), scRev3-RBM2 (residues 595–629), and scRev3-zipper (residues 573–594), were dialyzed overnight in ITC buffer, 50 mM Tris, 100 mM NaCl, pH 8.4. A stock solution of scRev3-RBM1 or scRev3-zipper peptide (300 μM) was titrated into MBP-scRev7 (30 μM) in 2.5 μl increments, while a stock of scRev3-RBM2 (150 μM) was titrated into 30 μM MBP-scRev7 in 2.0 μl increments (experiments were performed in triplicate). The data were fit using NanoAnalyze software to obtain dissociation constant (K_d), binding enthalpy (ΔH) and a stoichiometry parameter (n). Dilution ITC experiments with the scRev7/scRev3-RBM2 9xGS fusion construct were performed by titrating 450 μM protein dissolved in 50 mM Tris, 100 mM NaCl, pH 8.0 into the matching buffer.

Yeast 2-hybrid

Assays were performed using yeast strain PJ694-A. -LW broth was inoculated with competent yeast cells transformed with 2.0 ug of each of scRev7-AD and scRev3-BD, or scRev7-BD and scRev3-AD vector (scRev3 - RBM1, RBM2 or RBM12; WT or mutant) and incubated at 30 °C for 3 to 5 days (56). Empty vectors and AD- and BD-fused mRev7 undergoing dimerization (29) were used as negative and positive controls, respectively. Cells were pelleted and resuspended in sterile H_2O to normalize OD. Samples were serial diluted and plated onto -LW and -AHLW plates and incubated for 5 to 7 days at 30 °C.

Analytical ultracentrifugation

Sedimentation velocity analysis was conducted at 20 °C and 45,000 RPM using two channel aluminum-Epon double-sector centerpieces and quartz windows. Absorbance scans were acquired at 20 s intervals for 12 h at 20 °C with a Beckman-Coulter Optima AUC analytical ultracentrifuge. The rotor was equilibrated under vacuum at 20 °C for 1 h prior to start. The scans were analyzed using the c(s) distribution method in the Sedfit software (68). Partial specific volumes and solvent densities and viscosities were determined using SEDNTERP (69).

SAXS measurements and data analysis

Proteins were dialyzed into 2% glycerol, 20 mM Tris, 100 mM NaCl, pH 8. SAXS experiments were conducted at Brookhaven National Laboratory, LiX beamline and CHESS, ID7A1 beamline. Data collection parameters are summarized in Table S1. Guinier analysis, pair distance distribution P(r) analysis, Kratky analysis, and molecular weight calculations were performed using the software RAW (70). Theoretical SAXS data were generated using protein structures and evaluated with Crysol from the ATSAS software package (71). Molecular coordinates of scRev7/scRev3-RBM2 and scRev7/scRev3-RBM12 modules were extracted from PDB: 6V93. Missing residues and His-tags were modeled in with Modeller (72).

Data availability

Data generated in this study and included in the manuscript and supplementary materials are available upon request.

Supporting information—This article contains supporting information including Figures S1–S6 and Tables S1–S2.

Acknowledgments—The authors thank Dr Irina Bezsonova for helpful discussion and assistance with preparation of the manuscript graphics and Dr Jeremy L. Balsbaugh for assistance with proteomics analysis.

Author contributions—K. S. M., A. A. R., G. C. W., and D. M. K. conceived the research. K. S. M., A. A. R., H. E., N. C., and D. M. K. performed the research. K. S. M. and D. M. K. wrote the manuscript. All authors contributed to experiment design and manuscript preparation.

Funding and additional information—This work was supported by NSF MCB-1615866 and NIH NCI R01CA233959 grants to D. M. K. and by NIEHS R35ES028303 grant to G. C. W. G. C. W. is an American Cancer Society Professor. SAXS data were collected at the Center for High Energy X-ray Sciences (CHEXS), which is supported by NSF DMR-1829070 award, and the Macromolecular Diffraction at CHESS (MacCHESS) facility, which is supported by award NIH P30GM124166 grant and by New York State's Empire State Development Corporation (NYSTAR). This research also used the 16-ID LiX beamline of the National Synchrotron Light Source II, a U.S. Department of Energy (DOE) Office of Science User Facility operated for the DOE Office of Science by Brookhaven National Laboratory under Contract No. DE-SMC0012704. The manuscript content is solely the responsibility of the authors and does not necessarily represent the official views of the National Institutes of Health.

Conflict of interest—The authors declare that they have no conflicts of interest with the contents of this article.

Abbreviations—The abbreviations used are: AUC, analytical ultracentrifugation; AD, activation domain; BD, binding domain; -AHLW, plates lacking adenine, histidine, leucine, and tryptophan;

hRev7, Human Rev7; HORMA, Hop1, Rev7, Mad2; ITC, isothermal titration calorimetry; MBP-scRev7, scRev7 fused to the maltose binding protein; mRev7, mouse Rev7; RBM, Rev7-binding motif; SAXS, small-angle X-ray scattering; scPolζ, *S. cerevisiae* Polζ; SEC, size-exclusion chromatography; TLS, translesion synthesis; Y2H, yeast 2-hybrid.

References

1. Sale, J. E., Lehmann, A. R., and Woodgate, R. (2012) Y-family DNA polymerases and their role in tolerance of cellular DNA damage. *Nat. Rev. Mol. Cell Biol.* **13**, 141–152
2. Vaisman, A., and Woodgate, R. (2017) Translesion DNA polymerases in eukaryotes: what makes them tick? *Crit. Rev. Biochem. Mol. Biol.* **52**, 274–303
3. Chang, D. J., and Cimprich, K. A. (2009) DNA damage tolerance: when it's OK to make mistakes. *Nat. Chem. Biol.* **5**, 82–90
4. Shachar, S., Ziv, O., Avkin, S., Adar, S., Wittschieben, J., Reissner, T., *et al.* (2009) Two-polymerase mechanisms dictate error-free and error-prone translesion DNA synthesis in mammals. *EMBO J.* **28**, 383–393
5. Livneh, Z., Ziv, O., and Shachar, S. (2010) Multiple two-polymerase mechanisms in mammalian translesion DNA synthesis. *Cell Cycle* **9**, 729–735
6. Prakash, S., and Prakash, L. (2002) Translesion DNA synthesis in eukaryotes: a one- or two-polymerase affair. *Genes Dev.* **16**, 1872–1883
7. Hoege, C., Pfander, B., Moldovan, G. L., Pyrowolakis, G., and Jentsch, S. (2002) RAD6-dependent DNA repair is linked to modification of PCNA by ubiquitin and SUMO. *Nature* **419**, 135–141
8. Bienko, M., Green, C. M., Crosetto, N., Rudolf, F., Zapart, G., Coull, B., *et al.* (2005) Ubiquitin-binding domains in Y-family polymerases regulate translesion synthesis. *Science* **310**, 1821–1824
9. Kannouche, P. L., Wing, J., and Lehmann, A. R. (2004) Interaction of human DNA polymerase eta with monoubiquitinated PCNA: a possible mechanism for the polymerase switch in response to DNA damage. *Mol. Cell* **14**, 491–500
10. Martin, S. K., and Wood, R. D. (2019) DNA polymerase ζ in DNA replication and repair. *Nucl. Acids Res.* **47**, 8348–8361
11. Northam, M. R., Moore, E. A., Mertz, T. M., Binz, S. K., Stith, C. M., Stepchenkova, E. I., *et al.* (2014) DNA polymerases ζ and Rev1 mediate error-prone bypass of non-B DNA structures. *Nucl. Acids Res.* **42**, 290–306
12. Kochenova, O. V., Bezalel-Buch, R., Tran, P., Makarova, A. V., Chabes, A., Burgers, P. M., *et al.* (2017) Yeast DNA polymerase ζ maintains consistent activity and mutagenicity across a wide range of physiological dNTP concentrations. *Nucl. Acids Res.* **45**, 1200–1218
13. Northam, M. R., Robinson, H. A., Kochenova, O. V., and Shcherbakova, P. V. (2010) Participation of DNA polymerase zeta in replication of undamaged DNA in Saccharomyces cerevisiae. *Genetics* **184**, 27–42
14. Lazzaro, F., Novarina, D., Amara, F., Watt, D. L., Stone, J. E., Costanzo, V., *et al.* (2012) RNase H and postreplication repair protect cells from ribonucleotides incorporated in DNA. *Mol. Cell* **45**, 99–110
15. Moore, A., Dominska, M., Greenwell, P., Aksenova, A. Y., Mirkin, S., and Petes, T. (2018) Genetic control of genomic alterations induced in yeast by interstitial telomeric sequences. *Genetics* **209**, 425–438
16. Saini, N., Zhang, Y., Nishida, Y., Sheng, Z., Choudhury, S., Mieczkowski, P., *et al.* (2013) Fragile DNA motifs trigger mutagenesis at distant chromosomal loci in saccharomyces cerevisiae. *PLoS Genet.* **9**, e1003551
17. Tang, W., Dominska, M., Gawel, M., Greenwell, P. W., and Petes, T. D. (2013) Genomic deletions and point mutations induced in Saccharomyces cerevisiae by the trinucleotide repeats (GAA·TTC) associated with Friedreich's ataxia. *DNA Repair (Amst)* **12**, 10–17
18. Bhat, A., Andersen, P. L., Qin, Z., and Xiao, W. (2013) Rev3, the catalytic subunit of Polζ, is required for maintaining fragile site stability in human cells. *Nucl. Acids Res.* **41**, 2328–2339
19. Washington, M. T., and Gildenberg, M. S. (2020) Structure of DNA polymerase ζ: capturing the getaway driver. *Nat. Struct. Mol. Biol.* **27**, 1–2
20. Gómez-Llorente, Y., Malik, R., Jain, R., Choudhury, J. R., Johnson, R. E., Prakash, L., *et al.* (2013) The architecture of yeast DNA polymerase ζ. *Cell Rep.* **5**, 79–86
21. Johnson, R. E., Prakash, L., and Prakash, S. (2012) Pol31 and Pol32 subunits of yeast DNA polymerase δ are also essential subunits of DNA polymerase ζ. *Proc. Natl. Acad. Sci. U. S. A.* **109**, 12455–12460
22. Makarova, A. V., Stodola, J. L., and Burgers, P. M. (2012) A four-subunit DNA polymerase ζ complex containing Pol δ accessory subunits is essential for PCNA-mediated mutagenesis. *Nucl. Acids Res.* **40**, 11618–11626
23. Rizzo, A. A., and Korzhnev, D. M. (2019) The Rev1-Polζ translesion synthesis mutasome: structure, interactions and inhibition. *Enzymes* **45**, 139–181
24. Baranovskiy, A. G., Lada, A. G., Siebler, H. M., Zhang, Y., Pavlov, Y. I., and Tahirov, T. H. (2012) DNA polymerase δ and ζ switch by sharing accessory subunits of DNA polymerase δ. *J. Biol. Chem.* **287**, 17281–17287
25. Lee, Y. S., Gregory, M. T., and Yang, W. (2014) Human Pol ζ purified with accessory subunits is active in translesion DNA synthesis and complements Pol η in cisplatin bypass. *Proc. Natl. Acad. Sci. U. S. A.* **111**, 2954–2959
26. Makarova, A. V., and Burgers, P. M. (2015) Eukaryotic DNA polymerase ζ. *DNA Repair (Amst)* **29**, 47–55
27. Nelson, J. R., Lawrence, C. W., and Hinkle, D. C. (1996) Thymine-thymine dimer bypass by yeast DNA polymerase zeta. *Science* **272**, 1646–1649
28. Morrison, A., Christensen, R. B., Alley, J., Beck, A. K., Bernstine, E. G., Lemontt, J. F., *et al.* (1989) REV3, a Saccharomyces cerevisiae gene whose function is required for induced mutagenesis, is predicted to encode a nonessential DNA polymerase. *J. Bacteriol.* **171**, 5659–5667
29. Rizzo, A. A., Vassel, F. M., Chatterjee, N., D'Souza, S., Li, Y., Hao, B., *et al.* (2018) Rev7 dimerization is important for assembly and function of the Rev1/Polζ translesion synthesis complex. *Proc. Natl. Acad. Sci. U. S. A.* **115**, E8191–E8200
30. Tomida, J., Takata, K., Lange, S. S., Schibler, A. C., Yousefzadeh, M. J., Bhetawal, S., *et al.* (2015) REV7 is essential for DNA damage tolerance via two REV3L binding sites in mammalian DNA polymerase ζ. *Nucl. Acids Res.* **43**, 1000–1011
31. Hara, K., Shimizu, T., Unzai, S., Akashi, S., Sato, M., and Hashimoto, H. (2009) Purification, crystallization and initial X-ray diffraction study of human REV7 in complex with a REV3 fragment. *Acta Crystallogr. Sect. F Struct. Biol. Cryst. Commun.* **65**, 1302–1305
32. Hara, K., Hashimoto, H., Murakumo, Y., Kobayashi, S., Kogame, T., Unzai, S., *et al.* (2010) Crystal structure of human REV7 in complex with a human REV3 fragment and structural implication of the interaction between DNA polymerase zeta and REV1. *J. Biol. Chem.* **285**, 12299–12307
33. Acharya, N., Johnson, R. E., Prakash, S., and Prakash, L. (2006) Complex formation with Rev1 enhances the proficiency of Saccharomyces cerevisiae DNA polymerase zeta for mismatch extension and for extension opposite from DNA lesions. *Mol. Cell Biol.* **26**, 9555–9563
34. Malik, R., Kopylov, M., Gomez-Llorente, Y., Jain, R., Johnson, R. E., Prakash, L., *et al.* (2020) Structure and mechanism of B-family DNA polymerase ζ specialized for translesion DNA synthesis. *Nat. Struct. Mol. Biol.* **27**, 913–924
35. Du Truong, C., Craig, T. A., Cui, G., Botuyan, M. V., Serkasevich, R. A., Chan, K. Y., *et al.* (2021) Cryo-EM reveals conformational flexibility in apo DNA polymerase ζ. *J. Biol. Chem.* **297**, 100912
36. Kikuchi, S., Hara, K., Shimizu, T., Sato, M., and Hashimoto, H. (2012) Structural basis of recruitment of DNA polymerase ζ by interaction between REV1 and REV7 proteins. *J. Biol. Chem.* **287**, 33847–33852
37. Pustovalova, Y., Bezsonova, I., and Korzhnev, D. M. (2012) The C-terminal domain of human Rev1 contains independent binding sites for DNA polymerase η and Rev7 subunit of polymerase ζ. *FEBS Lett.* **586**, 3051–3056
38. Wojtaszek, J., Liu, J., D'Souza, S., Wang, S., Xue, Y., Walker, G. C., *et al.* (2012) Multifaceted recognition of vertebrate Rev1 by translesion polymerases ζ and κ. *J. Biol. Chem.* **287**, 26400–26408
39. Aravind, L., and Koonin, E. V. (1998) The HORMA domain: a common structural denominator in mitotic checkpoints, chromosome synapsis and DNA repair. *Trends Biochem. Sci.* **23**, 284–286

40. Rosenberg, S. C., and Corbett, K. D. (2015) The multifaceted roles of the HORMA domain in cellular signaling. *J. Cell Biol.* **211**, 745–755
41. de Krijger, I., Boersma, V., and Jacobs, J. J. L. (2021) REV7: jack of many trades. *Trends Cell Biol.* **31**, 686–701
42. Luo, X., Fang, G., Coldiron, M., Lin, Y., Yu, H., Kirschner, M. W., *et al.* (2000) Structure of the Mad2 spindle assembly checkpoint protein and its interaction with Cdc20. *Nat. Struct. Biol.* **7**, 224–229
43. Luo, X., Tang, Z., Xia, G., Wassmann, K., Matsumoto, T., Rizo, J., *et al.* (2004) The Mad2 spindle checkpoint protein has two distinct natively folded states. *Nat. Struct. Mol. Biol.* **11**, 338–345
44. Dai, Y., Zhang, F., Wang, L., Shan, S., Gong, Z., and Zhou, Z. (2020) Structural basis for shieldin complex subunit 3-mediated recruitment of the checkpoint protein REV7 during DNA double-strand break repair. *J. Biol. Chem.* **295**, 250–262
45. Wang, X., Pernicone, N., Pertz, L., Hua, D., Zhang, T., Listovsky, T., *et al.* (2019) REV7 has a dynamic adaptor region to accommodate small GTPase RAN/Shigella IpaB ligands, and its activity is regulated by the RanGTP/GDP switch. *J. Biol. Chem.* **294**, 15733–15742
46. Hara, K., Taharazako, S., Ikeda, M., Fujita, H., Mikami, Y., Kikuchi, S., *et al.* (2017) Dynamic feature of mitotic arrest deficient 2-like protein 2 (MAD2L2) and structural basis for its interaction with chromosome alignment-maintaining phosphoprotein (CAMP). *J. Biol. Chem.* **292**, 17658–17667
47. Liang, L., Feng, J., Zuo, P., Yang, J., Lu, Y., and Yin, Y. (2020) Molecular basis for assembly of the shieldin complex and its implications for NHEJ. *Nat. Commun.* **11**, 1972
48. Noordermeer, S. M., Adam, S., Setiaputra, D., Barazas, M., Pettitt, S. J., Ling, A. K., *et al.* (2018) The shieldin complex mediates 53BP1-dependent DNA repair. *Nature* **560**, 117–121
49. Gupta, R., Somyajit, K., Narita, T., Maskey, E., Stanlie, A., Kremer, M., *et al.* (2018) DNA repair network analysis reveals shieldin as a key regulator of NHEJ and PARP Inhibitor sensitivity. *Cell* **173**, 972–988
50. Gao, S., Feng, S., Ning, S., Liu, J., Zhao, H., Xu, Y., *et al.* (2018) An OB-fold complex controls the repair pathways for DNA double-strand breaks. *Nat. Commun.* **9**, 3925
51. Ghezraoui, H., Oliveira, C., Becker, J. R., Bilham, K., Moralli, D., Anzilotti, C., *et al.* (2018) 53BP1 cooperation with the REV7-shieldin complex underpins DNA structure-specific NHEJ. *Nature* **560**, 122–127
52. Setiaputra, D., and Durocher, D. (2019) Shieldin - the protector of DNA ends. *EMBO Rep.* **20**, e47560
53. Drozdetskiy, A., Cole, C., Procter, J., and Barton, G. J. (2015) JPred4: a protein secondary structure prediction server. *Nucl. Acids Res.* **43**, W389–394
54. Shen, X. X., Opulente, D. A., Kominek, J., Zhou, X., Steenwyk, J. L., Buh, K. V., *et al.* (2018) Tempo and mode of genome evolution in the budding yeast subphylum. *Cell* **175**, 1533–1545
55. Doig, A. J., and Baldwin, R. L. (1995) N- and C-capping preferences for all 20 amino-acids in alpha-helical peptides. *Protein Sci.* **4**, 1325–1336
56. James, P., Halladay, J., and Craig, E. A. (1996) Genomic libraries and a host strain designed for highly efficient two-hybrid selection in yeast. *Genetics* **144**, 1425–1436
57. Krissinel, E., and Henrick, K. (2007) Inference of macromolecular assemblies from crystalline state. *J. Mol. Biol.* **372**, 774–797
58. Svergun, D., Barberato, C., and Koch, M. H. (1995) CRYSOL–a program to evaluate X-ray solution scattering of biological macromolecules from atomic coordinates. *J. Appl. Crystallogr.* **28**, 768–773
59. Hammel, M. (2012) Validation of macromolecular flexibility in solution by small-angle X-ray scattering (SAXS). *Eur. Biophys. J.* **41**, 789–799
60. Lange, S. S., Wittschieben, J. P., and Wood, R. D. (2012) DNA polymerase zeta is required for proliferation of normal mammalian cells. *Nucl. Acids Res.* **40**, 4473–4482
61. Clairmont, C. S., Sarangi, P., Ponnienselvan, K., Galli, L. D., Csete, I., Moreau, L., *et al.* (2020) TRIP13 regulates DNA repair pathway choice through REV7 conformational change. *Nat. Cell Biol.* **22**, 87–96
62. Sarangi, P., Clairmont, C. S., Galli, L. D., Moreau, L. A., and D'Andrea, A. D. (2020) p31(comet) promotes homologous recombination by inactivating REV7 through the TRIP13 ATPase. *Proc. Natl. Acad. Sci. U. S. A.* **117**, 26795–26803
63. Corbett, K. D. (2020) p31(comet) and TRIP13 recycle Rev7 to regulate DNA repair. *Proc. Natl. Acad. Sci. U. S. A.* **117**, 27761–27763
64. Madeira, F., Park, Y. M., Lee, J., Buso, N., Gur, T., Madhusoodanan, N., *et al.* (2019) The EMBL-EBI search and sequence analysis tools APIs in 2019. *Nucleic Acids Res.* **47**, W636–W641
65. The PyMOL Molecular Graphics System, Version 1.8, Schrödinger LLC.
66. Erster, O., and Liscovitch, M. (2010) A modified inverse PCR procedure for insertion, deletion, or replacement of a DNA fragment in a target sequence and its application in the ligand interaction scan method for generation of ligand-regulated proteins. *Met. Mol. Biol.* **634**, 157–174
67. Cox, J., and Mann, M. (2008) MaxQuant enables high peptide identification rates, individualized p.p.b.-range mass accuracies and proteome-wide protein quantification. *Nat. Biotechnol.* **26**, 1367–1372
68. Schuck, P. (2000) Size-distribution analysis of macromolecules by sedimentation velocity ultracentrifugation and lamm equation modeling. *Biophys. J.* **78**, 1606–1619
69. Laue, T. M., Shah, B., Ridgeway, T. M., and Pelletier, S. L. (1992) Computer-aided interpretation of analytical sedimentation data for proteins. In: Harding, S. E., Rowe, A. J., Horton, J. C., eds. *Analytical Ultracentrifugation in Biochemistry and Polymer Science* (pp. 90–125). Cambridge
70. Hopkins, J. B., Gillilan, R. E., and Skou, S. (2017) BioXTAS RAW: improvements to a free open-source program for small-angle X-ray scattering data reduction and analysis. *J. Appl. Crystallogr.* **50**, 1545–1553
71. Franke, D., Petoukhov, M. V., Konarev, P. V., Panjkovich, A., Tuukkanen, A., Mertens, H. D. T., *et al.* (2017) Atsas 2.8: a comprehensive data analysis suite for small-angle scattering from macromolecular solutions. *J. Appl. Crystallogr.* **50**, 1212–1225
72. Webb, B., and Sali, A. (2016) Comparative protein structure modeling using MODELLER. *Curr. Protoc. Bioinform.* **54**. https://doi.org/10.1002/0471250953.bi0506s47